



1 **The possibility of rainfall estimation using $R(Z, Z_{DR}, K_{DP}, A_H)$:**
2 **A case study of heavy rainfall on 25 August 2014 in Korea**

3

4 **C.-H. You¹, M.-Y. Kang² and D.-I. Lee^{1,2}**

5 [1]{Atmospheric Environmental Research Institute, Pukyong National University, Busan,
6 South Korea}

7 [2]{Department of Environmental Atmospheric Sciences, Pukyong National University,
8 Busan, South Korea}

9 Correspondence to: D.-I. Lee (leedi@pknu.ac.kr)

10

11 **Abstract**

12 To improve the accuracy of polarimetric rainfall relations for heavy rainfall, an extreme
13 rainfall case was analysed and some methods were examined. The observed differential
14 reflectivity (Z_{DR}) quality check was theoretically investigated using the relation between the
15 standard deviation of differential reflectivity and cross correlation, and the light rain method
16 for Z_{DR} bias was also applied to the rainfall estimation. The best performance for this heavy
17 rainfall case was obtained when the moving average of Z_{DR} over a window size of 9 gates was
18 applied to the rainfall estimation using horizontal reflectivity (Z_H) and Z_{DR} and to the
19 calculation of Z_H bias. The differential reflectivity calculated by disdrometer data may be an
20 alternative to the vertical pointing scan for calculating Z_{DR} bias. The accuracy of the
21 combined rainfall relation, $R(Z, Z_{DR}, K_{DP}, A_H)$ was relatively insensitive to Z_{DR} and Z_H biases in
22 both observations and simulations.

23

24 **1 Introduction**

25 Weather radar is a very useful remote sensing instrument for estimating rainfall amount due to
26 its high spatial and temporal resolution compared with other instruments. Calculations of
27 radar rainfall are based on the relationship between reflectivity (Z) and rain rate (R) known as
28 the Z - R relation (hereafter $R(Z)$). Experimentally measured drop size distributions (DSDs)
29 have been extensively used to obtain both radar reflectivity and rain rate (Compos and



1 Zawadzki, 2000). It can be shown that there is no unique global $R(Z)$ relation because DSDs
2 can vary from storm to storm and even within the storm itself (You et al., 2010). There have
3 been a few studies on the calculation of the $R(Z)$ relationship using disdrometer data with
4 rainfall types and rain gage adjusted rainfall amount for operational Doppler weather radars in
5 Korea (Jang et al., 2004; You et al., 2004; Suk et al., 2005).

6 Radar rainfall estimation may be contaminated by uncertainties such as hardware calibration,
7 partial beam filling, rain attenuation, bright band, and non-weather echoes (Wilson and
8 Brandes, 1979; Austin, 1989). To mitigate these problems, particle identification algorithms
9 have been developed using polarimetric parameters for improving data quality control and
10 rainfall estimates by discriminating non-meteorological artefacts such as anomalous
11 propagation, birds, insects, second trip echo, and melting layer detection (Ryzhkov and Zrnica,
12 1998; Vivekanandan et al., 1999; Giangrande et al., 2008). The improvement of radar rainfall
13 accuracy is a major reason for using polarimetric radar (Ryzhkov and Zrnica, 1996; May et al.,
14 1999; Bringi and Chandrasekar, 2001). Ryzhkov et al. (2005a) developed a rainfall algorithm
15 using polarimetric radar for the prototype WSR-88D (Weather Surveillance Radar-88 Doppler)
16 system using different drop shape assumptions. Cifelli et al. (2011) compared two rainfall
17 algorithms, CSU-HIDRO (Colorado State University-Hydrometeor IDentification of Rainfall)
18 and JPOLE (Joint Polarization Experiment)-like, in the high plains environment. Ryzhkov et
19 al. (2014) recently investigated the potential use of specific attenuation (A_H) for rainfall
20 estimation with X-band and S-band radar and found that the $R(A_H)$ method yields robust
21 estimates of rain rates even at S band where attenuation is very small.

22 As a result of these theoretical and other experimental studies, many countries are replacing or
23 modifying their radars and using polarimetric radar operationally. There are three major
24 agencies that operate radars to monitor and forecast severe weather and flash flooding
25 operationally in Korea: the Ministry of National Defense (MND), the Ministry of Land,
26 Infrastructure and Transportation (MoLIT), and the Korea Meteorological Administration
27 (KMA), with the MoLIT the first to install polarimetric radars in Korea. The KMA installed
28 an S-band polarimetric radar in the far northwest of Korea in 2014. For successful operational
29 implementation of these radars, considerable research on rainfall estimation, hydrometeor
30 classification, and DSD retrieval is required. However, there have been few studies on these
31 polarimetric related issues other than the derivation of relationships using long period
32 disdrometer data and the assessment of each relation after applying a very simple quality



1 control for differential phase shift (You et al., 2014). You et al. (2014) found that the accuracy
2 of rainfall estimation using horizontal reflectivity (Z_H) and differential reflectivity (Z_{DR})
3 obtained by DSDs in the Busan area in Korea was better than that obtained with relations
4 calculated by DSDs measured in Oklahoma in the US. A quality control algorithm and
5 unfolding of differential phase shift (Φ_{DP}) for calculating specific differential phase (K_{DP})
6 were applied to the rainfall estimation (You et al., 2014). Recently, You et al. (2015a)
7 proposed a relation combining many polarimetric variables of the form $R(Z, Z_{DR}, K_{DP}, A_H)$ as a
8 candidate for an optimum rainfall relation for S-band polarimetric data in Korea; this would
9 allow a single relation to be used for different hydrometeor regimes in the absence of a stable
10 hydrometeor classification algorithm. However, there are still issues to be resolved in
11 improving Z_{DR} data quality and the robustness of $R(Z, Z_{DR}, K_{DP}, A_H)$ for the heavy rainfall case
12 where error propagation from each polarimetric variable can occur.

13 This paper discusses how to improve the accuracy of rainfall estimation using moving
14 averaged differential reflectivity and examines the robustness of the $R(Z, Z_{DR}, K_{DP}, A_H)$ relation
15 for a heavy rainfall case in Korea. Sect. 2 describes the rain gage, DSD and radar dataset,
16 together with the calculation of polarimetric variables from DSDs and the validation methods.
17 Sect. 3 provides Z_H and Z_{DR} bias correction, an examination of Z_{DR} data quality, and the
18 statistical results of rainfall estimation using observed and moving-average Z_{DR} . Sect. 4
19 contains a discussion of a possible method for improving $R(Z, Z_{DR})$ accuracy and the
20 robustness of the $R(Z, Z_{DR}, K_{DP}, A_H)$ relation. Finally, we provide some conclusions in Sect. 5.

21

22 **2 Data and methodology**

23 **2.1 Gage, disdrometer and radar dataset**

24 The rainfall data from rain gages operated by the KMA were used to evaluate the accuracy of
25 radar rainfall. Rain gages located within the radar coverage area at distances from 5 to 95 km
26 of the radar are included in the analysis. Fig. 1 shows the location of all instruments used in
27 this study. The circle is the radar coverage, the solid rectangle is the centre of the Bislsan
28 radar, the plus signs show the rain gages within the radar coverage and the open rectangle is
29 the location of a PARSIVEL (PARticle Size VELOCITY) and POSS (Precipitation Occurrence



1 Sensor System; detailed specifications are provided by Sheppard, 1990) disdrometer installed
2 ~82 km away from the radar.

3 Relations for converting radar variables into rain rate are required because the radar does not
4 observe rainfall directly. To calculate these relations, disdrometer data that can measure the
5 DSDs are needed. One-min DSDs obtained by the POSS from 2001 to 2004 were used. To
6 improve the accuracy of Z_{DR} , DSDs observed by PARSIVEL on 25 August 2014 were used
7 because POSS data were not available at that time. The PARSIVEL disdrometer is a laser-
8 optic system that measures 32 channels from 0.062 to 24.5 mm (detailed specifications are
9 given by Löffler-Mang and Joss, 2000).

10 Unreliable data, defined as belonging to the following categories, were removed: 1-min rain
11 rate less than 0.1 mm h^{-1} ; total number concentrations of all channels less than 10; drop
12 numbers counted only in the lower 10 channels (0.84 mm for POSS and 1.187 mm for
13 PARSIVEL); and drop numbers counted only in the lower 5 channels (0.54 mm for POSS and
14 0.562 mm for PARSIVEL) (You et al., 2015b).

15 Radar data were collected by the Bislan polarimetric radar installed and operated by the
16 MoLIT in Korea since 2009. The transmitted peak power is 750 kW, beam width is 0.95° , and
17 frequency is 2.791 GHz. The polarimetric variables are estimated with a gate size of 0.125 km.
18 The scan strategy is composed of 6 elevation angles with 2.5-min update interval.
19 Polarimetric variables for 0.5° elevation angle were extracted from the volume data every 10
20 mins for this study.

21 2.2 Calculation of polarimetric variables from DSDs

22 Polarimetric variables were calculated using T-matrix scattering techniques derived by
23 Waterman (1971) and later developed further by Mishchenko et al. (1996). The following
24 raindrop shape assumptions are used for the calculation of variables from the DSDs:

$$25 \frac{b}{a} = 1.0048 + 0.500057 D - 0.02628 D^2 + 0.003682 D^3 - 0.0001677 D^4, \quad (1)$$

$$26 \frac{b}{a} = 1.012 - 0.01445 D - 0.01028 D^2, \quad (2)$$

27 where a, b and D are the major axis, minor axis, and equi-volume diameter of raindrop in
28 millimetres, respectively.



1 Eq. (1) is for the equilibrium axis ratio derived from the numerical model of Beard and Chung
 2 (1987), which is in good agreement with the results from wind tunnel measurements. The
 3 actual shapes of raindrops in turbulent flow are expected to be different from the equilibrium
 4 shapes due to drop oscillations. Oscillating drops appear to be more spherical on average than
 5 drops with equilibrium shapes as shown by Andsager et al. (1999) in laboratory studies. They
 6 demonstrated that the shape of raindrops with diameter between 1.1 and 4.4 mm is better
 7 explained by Eq. (2). You et al. (2015a) found that combining Eq. (1) for drops less than 1.1
 8 mm and larger than 4.4 mm with Eq. (2) for the drop diameter between 1.1 and 4.4 mm as
 9 proposed by Brangi et al. (2003) gave the best rainfall estimation compared with other drop
 10 axis ratio assumptions in Korea, and we use this combined formulation in this study. Other
 11 parameters in the T-matrix calculations include the temperature, which is assumed to be 20°C
 12 in this study. The distribution of canting angles of raindrops is Gaussian with a mean of 0°
 13 and a standard deviation of 7°, as determined recently by Huang et al. (2008).

14 2.3 Validation

15 The localized rainfall on 25 August 2014 was caused by a low pressure system that passed
 16 through southern Korea. Fig. 2 shows the time series of hourly rainfall and accumulated
 17 rainfall from the three gages, ID 255 (North Changwon site), ID 926 (Jinbook site), and ID
 18 939 (Geumjeong-gu site) that recorded the highest rainfall within the radar coverage area. The
 19 daily accumulated rainfall values were 243.5 mm, 269.0 mm, and 244.5 mm for these gages.
 20 The time period analysed was from 0900 LT to 1600 LT because the rainfall was
 21 concentrated in this period and radar data were available from 0900 LT.

22 The normalized error (NE), fractional root mean square error (RMSE), and correlation
 23 coefficients (CC) of the rainfall relations and 121 gages were used to investigate the
 24 performance of each rainfall relation:

$$25 \quad NE = \frac{\frac{1}{N} \sum_{i=1}^N |R_{R,i} - R_{G,i}|}{R_G}, \quad (3)$$

$$26 \quad RMSE = \left[\frac{1}{N} \sum_{i=1}^N (R_{R,i} - R_{G,i})^2 \right]^{1/2}, \quad (4)$$



$$1 \quad CC = \frac{\sum_{i=1}^N (R_{R,i} - \overline{R_R})(R_{G,i} - \overline{R_G})}{\left[\sum_{i=1}^N (R_{R,i} - \overline{R_R})^2 \right]^{1/2} \left[\sum_{i=1}^N (R_{G,i} - \overline{R_G})^2 \right]^{1/2}}, \quad (5)$$

2 where N is the number of radar rainfall (R_R) and gage rainfall (R_G) pairs, and $\overline{R_R}$ and $\overline{R_G}$ are
 3 the average hourly rain rates from the radar and gage, respectively. These statistical variables
 4 are calculated using hourly rainfall amounts derived from the radar and gage at the location of
 5 the gage. The radar rainfall at the rain gage was obtained by averaging rainfall over a small
 6 area (1 km \times 1°) centered on each rain gage. The rainfall relations for calculating radar
 7 rainfall were obtained from the simulated polarimetric variables generated from DSDs and are
 8 summarized in Table 1.

9

10 **3 Results**

11 **3.1 Improvement of Z_{DR} data quality**

12 Z_{DR} is an important variable for hydrometeor classification and rainfall estimation. To check
 13 the quality of the Z_{DR} measurements, the radial profile of Z_{DR} was investigated as shown in
 14 Fig. 3. Fig. 3(a) shows the spatial distribution of Z_{DR} at 0.5° elevation at 1401 LT on 25
 15 August 2014. Fig. 3(b) shows the radial profile of observed Z_{DR} (red line) and the standard
 16 deviation of Z_{DR} (black line) calculated using 9 gates along the line A–B shown in Fig. 3(a).
 17 The average standard deviation of Z_{DR} along the line was 0.615 dB. Fig. 3(c) shows the radial
 18 profile of the cross correlation; the average cross correlation was 0.982.

19 To find the accuracy of the observed Z_{DR} value, we use the theoretical relation between the
 20 standard deviation of Z_{DR} and the cross correlation following Bring and Chandrasekar (2003):

$$21 \quad SD(Z_{DR}) = 10 \log_{10} \left\{ 1 + \left[\frac{2}{N} (1 - |\rho_{co}|^2) \sum_{l=-(N-1)}^{N-1} \left(1 - \frac{|l|}{N} \right) |\rho_{co}(l)|^2 \right]^{1/2} \right\}, \quad (6)$$

22 where $SD(Z_{DR})$ is standard deviation of Z_{DR} , N is the number of samples and ρ_{co} is the cross
 23 correlation, given by



$$\rho[n] = \exp\left(-\frac{8\pi^2\sigma_v^2 n^2 T_s^2}{\lambda^2}\right), \quad (7)$$

2 where ρ is the cross correlation, σ_v is Doppler width, n is sample number, and T_s is dwell
3 time.

4 For a better comparison we display the correlations in L space, as proposed by Keat et al.
5 (2015)

$$L = -10 \log_{10}(1 - \rho_{nv}), \quad (8)$$

7 where, ρ_{nv} is cross correlation. Fig. 4 shows the theoretical relation between the standard
8 deviation of Z_{DR} and the cross correlation coefficient. Fig. 4(a) shows the results obtained
9 using the scan configuration of the Bislan radar. The dwell time is 56 ms, number of samples
10 is 55, and the normalised Doppler width is 0.02. Fig. 4(a) suggests that for an accuracy of 0.1
11 dB in Z_{DR} with 1 ms^{-1} Doppler width, a value of L of over 3 ($\rho_{nv} > 0.999$) is needed. Such
12 values cannot be measured with the antenna. In Fig. 4(b) the number of samples is 495, which
13 corresponds to 9 gates, 1.125 km in range; an accuracy of 0.2 dB in Z_{DR} (the moving-average
14 Z_{DR} , hereafter mZ_{DR}) is achieved with 1 ms^{-1} Doppler width and a value of L of 1.7 (ρ_{nv}
15 > 0.980).

16 Fig. 5 shows the results for Z_{DR} measurements at 1401 LT on 25 August 2014. Fig. 5(a)
17 shows the spatial distribution of a moving average Z_{DR} from 9 gates. Fig. 5(b) shows the
18 radial profile of the Z_{DR} (red line) and its standard deviation (black line) calculated for 9 gates
19 along the line A–B shown in Fig. 5(a). The average standard deviation of Z_{DR} along the ray
20 was 0.169 dB. Fig. 5(c) shows the radial profile of the cross correlation; the average cross
21 correlation was 0.985. Both the standard deviation of Z_{DR} and the averaged ρ_{nv} values are
22 very close to the theoretical values (standard deviation of Z_{DR} is 0.160 and ρ_{nv} is 0.987) as
23 shown in Fig. 4. Therefore, in the next Sect. a 9-gage moving average Z_{DR} was used for
24 absolute Z_H bias correction and rainfall estimation, and its effect on the accuracy of radar
25 rainfall estimation was examined.



1 **3.2 Absolute bias correction of Z_{DR} and Z_H**

2 Before calculating radar rainfall, the Z_H and Z_{DR} must be corrected for system bias. Ryzhkov
3 et al. (2005) calculated the required accuracy for classifying light rain and dry snow to be 1
4 dB and 0.2 dB for Z_H and Z_{DR} , respectively. The Z_{DR} bias correction is important for the
5 absolute calibration of the radar using the self-consistency method. Gorgucci et al. (1999)
6 proposed a vertical pointing scan of light rain to take advantage of the nearly spherical shape
7 of the raindrops seen from below.

8 Ryzhkov et al. (2005b) used the elevation angle dependency of Z_{DR} as an alternative
9 technique and concluded that the high variability of Z_{DR} in rainfall means it is not possible to
10 achieve the required absolute calibration of 0.2 dB. They also proposed a method using the
11 structural characteristics of the melting layer in stratiform clouds and measured the dry
12 aggregated snow present above the melting layer, which gave a mean value of 0.2 dB at S
13 band and an accuracy of 0.1 to 0.2 dB.

14 Trabal et al. (2009) evaluated two different methods using the intrinsic properties of dry
15 aggregated snow present above the melting layer and measurements of light rain close to the
16 ground and found that a Z_{DR} calibration accuracy of 0.2 dB or less was achieved for both
17 events analysed when both methods are compared.

18 The vertical pointing data were not available for the case considered here and the scan
19 strategy with six elevation angles does not detect the melting layer. Therefore, light rain
20 measurements close to the ground were used to calibrate the Z_{DR} and Z_H biases using the self-
21 consistency method in this study. Very light rain was defined by the thresholds $20 \text{ dBZ} \leq Z_H$
22 $\leq 28 \text{ dBZ}$ as proposed by Marks et al. (2011). The Z_H bias was determined following
23 Ryzhkov et al. (2005b).

24 The Z_H biases calculated with the self-consistency method using observed Z_{DR} and mZ_{DR} are
25 -1.95 dB and -1.48 dB , respectively. The Z_{DR} biases calculated by the very light rain method
26 using observed Z_{DR} (0.26 dB) and mZ_{DR} (0.3 dB), respectively.

27 **3.3 Validation**

28 To investigate the performance of $R(Z, Z_{DR})$ and $R(Z, Z_{DR}, K_{DP}, A_H)$, which is related to the Z_H
29 and Z_{DR} bias, NE, RMSE, and CC were calculated using hourly rainfall from each relation



1 and from the gages. For the comparison of rainfall amount, two different Z_H and Z_{DR} biases
2 were applied to observed variables as mentioned in Sect. 3.2. Each bias was calculated using
3 observed Z_{DR} and mZ_{DR} .

4 Fig. 6 shows the scatter plot of 1 hour rainfall obtained using $R(Z, Z_{DR})$ and gage data. In Fig.
5 6 (a) the Z_H bias was obtained from the observed Z_{DR} bias and the Z_{DR} biases calculated from
6 observed Z_{DR} (blue full circles) and mZ_{DR} (red full circles). The RMSE, NE, and CC of the
7 relation using mZ_{DR} were as much as 8 mm h^{-1} , 0.1, and 0.18 better than those obtained using
8 observed Z_{DR} , respectively. In Fig. 6(b) the Z_H bias is calculated from mZ_{DR} ; the improved
9 performance using mZ_{DR} is clear. The accuracy of the rainfall estimate using Z_H bias obtained
10 by mZ_{DR} is statistically more robust than that for the estimate based on observed Z_{DR} . The
11 RMSE, NE, and CC for the comparison of $R(Z, Z_{DR})$ rainfall obtained using different Z_H and
12 Z_{DR} biases are summarized in Table 2.

13 Fig. 7 shows the scatter plots when $R(Z, Z_{DR}, K_{DP}, A_H)$ is used for rainfall estimation. Fig. 7(a)
14 shows the radar rainfall calculated using the Z_H bias obtained from the observed Z_{DR} bias and
15 the Z_{DR} biases obtained from observed Z_{DR} (blue full circles) and mZ_{DR} (red full circles). The
16 RMSE, NE, and CC from each relation were not very different; differences of RMSE, NE,
17 and CC in the two cases were 0.2 mm h^{-1} , 0.01, and 0, respectively. The statistics for the
18 comparison of radar rainfall obtained using different Z_H and Z_{DR} biases are summarized in
19 Table 3. These results show that $R(Z, Z_{DR}, K_{DP}, A_H)$ is less sensitive to Z_H and Z_{DR} error than
20 $R(Z, Z_{DR})$. This will be discussed further in Sect. 4.2 using simulated data.

21

22 4 Discussion

23 4.1 Impact of disdrometer data on radar rainfall

24 In the cases described in Sect. 3.3, the accuracy of the $R(Z, Z_{DR})$ relation was improved when
25 the moving-average Z_{DR} (i.e., mZ_{DR}) was used to estimate rainfall. To improve the accuracy of
26 rainfall estimation using $R(Z, Z_{DR})$, we examined the impact of Z_{DR} bias (as obtained from
27 disdrometer data) on the accuracy. The DSD data were quality controlled and polarimetric
28 variables were calculated by T-matrix simulation with the same configuration as in Sect. 2.
29 Before applying the DSDs to rainfall estimation, 10-min rainfall amounts obtained by DSDs
30 and gages were compared.



1 Fig. 8 shows the scatter plot of 10-min rainfall amount measured by PARSIVEL and the gage
2 located less than 100 m away from PARSIVEL. The daily accumulated rainfall amounts were
3 116.0 mm for the gage and 129.4 mm for PARSIVEL. The RMSE, NE, and CC were 0.52
4 mm, 0.26, and 0.99, respectively. For the comparison the Z_{DR} of the radar was averaged over
5 $3 \text{ km} \times 3^\circ$ as shown in Fig. 9. The calculated Z_{DR} biases were 0.26 dB for observed Z_{DR} and
6 0.30 dB for mZ_{DR} . The Z_H biases described in Sect. 3.3 were used.

7 Fig. 10 shows the scatter plots of 1-hour rainfall obtained by $R(Z, Z_{DR})$ and gages. The radar
8 rainfall was calculated after Z_{DR} bias correction using the bias result in the comparison
9 between radar Z_{DR} and PARSIVEL Z_{DR} . The Z_{DR} biases were -0.05 dB for observed Z_{DR} and
10 -0.07 dB for mZ_{DR} . In Fig. 10 (a) the Z_H bias was obtained from the observed Z_{DR} bias and
11 Z_{DR} biases calculated from observed Z_{DR} (blue full circle) and mZ_{DR} (red full circle). The
12 radar rainfall using mZ_{DR} was better than that using observed Z_{DR} by as much as 5.5 mm h^{-1}
13 for RMSE and 0.36 for NE. In Fig. 10 (b) the Z_H bias was calculated from mZ_{DR} ; the
14 improved rainfall estimation using mZ_{DR} is clear. This result shows the better scores
15 compared with the statistics shown in Fig. 6 that were obtained using Z_{DR} biases extracted
16 from the radar Z_{DR} only. When the observed Z_{DR} , which fluctuates considerably along the ray,
17 was applied to the rainfall estimation, the rainfall amount was much more variable with Z_H
18 bias values (blue full circle) than that with mZ_{DR} (red circle) as shown in Fig. 10 (a) and (b).
19 According to these results, when moving average Z_{DR} (i.e., mZ_{DR}) is used with the Z_{DR} bias
20 measured by PARSIVEL, the accuracy of rainfall estimation was improved and was more
21 stable than that of other configurations using $R(Z, Z_{DR})$.

22 Fig. 11 shows the scatter plots for $R(Z, Z_{DR}, K_{DP}, A_H)$ and gages. The statistical scores were not
23 very different from Z_H and Z_{DR} biases. The differences of RMSE, NE, and CC between each
24 relation were 0.4 mm h^{-1} , 0.01, and 0, respectively. These results were summarized in Table 3.

25 4.2 Simulation of $R(Z, Z_{DR}, K_{DP}, A_H)$ with error propagation from each variable

26 With the relation using combined polarimetric variables, $R(Z, Z_{DR}, K_{DP}, A_H)$, error propagation
27 can affect the accuracy of radar rainfall estimation. To examine the contribution of errors
28 from each variable, simulated polarimetric variables such as Z , Z_{DR} , K_{DP} , A_H , were generated
29 with dimensions of 960 sizes of bins and 360 radials.

30 Fig. 12 shows the distribution function of the polarimetric variables generated assuming a
31 Gaussian distribution in each case. Fig. 12(a) shows the occurrence frequency of Z_H generated



1 with standard deviation of 7.0 dBZ and mean of 30.0 dBZ. Fig. 12(b) shows the
 2 corresponding occurrence frequency of Z_{DR} with 0.5 dB standard deviation and 1.0 dB mean.
 3 Fig. 12(c) shows the occurrence frequency of K_{DP} generated with $0.5^\circ \text{ km}^{-1}$ standard
 4 deviation and $1.0^\circ \text{ km}^{-1}$ mean. Fig. 12 (d) shows the occurrence frequency of A_H generated
 5 with $0.01^\circ \text{ km}^{-1}$ standard deviation and $0.0003^\circ \text{ km}^{-1}$ mean.

6 To investigate the extent of contamination of the rainfall amount by propagation of errors in
 7 each polarimetric variable for $R(Z, Z_{DR}, K_{DP}, A_H)$, the errors of Z , Z_{DR} , and K_{DP} ingested to
 8 simulated data were 0 to 5 dBZ with interval 0.25 dBZ, 0 to 0.6 dB with interval 0.03 dB, and
 9 0 to 0.2 degree km^{-1} with interval 0.01 degree km^{-1} , respectively. The rain rate was calculated
 10 by same $R(Z, Z_{DR}, K_{DP}, A_H)$ as applied to real data in the previous Sect.. The RMSE and NE
 11 were calculated for rainfall amount with and without error-ingested polarimetric variables.
 12 The rainfall amount obtained using the raw simulated variables was used as a reference.

13 Fig. 13 shows the RMSE and NE distribution of different polarimetric rainfall relations with
 14 ingested error. The magenta, black, red, green, blue, and purple lines show RMSE and NE
 15 obtained by the rainfall relations $R(Z)$, $R(K_{DP})$, $R(Z, K_{DP}, A_H)$, $R(Z, Z_{DR})$, $R(K_{DP}, Z_{DR})$, and
 16 $R(Z, Z_{DR}, K_{DP}, A_H)$, respectively. The threshold rainfall was from 0 to 300 mm h^{-1} for
 17 calculating statistical scores. Fig. 13(a) shows the RMSE distribution of each rainfall relation
 18 with different ingested error step. The RMSE of $R(Z, K_{DP}, A_H)$ is the largest of all the rainfall
 19 relations. The RMSE of $R(Z, Z_{DR}, K_{DP}, A_H)$ is higher than that of $R(Z)$, $R(Z, Z_{DR})$, and
 20 $R(K_{DP}, Z_{DR})$ but less than that of $R(K_{DP})$. It means that not all errors from Z , Z_{DR} , and K_{DP}
 21 propagate into the $R(Z, Z_{DR}, K_{DP}, A_H)$. Fig. 13(b) shows the corresponding distributions for NE.
 22 The value of NE increases in the order $R(Z, Z_{DR}, K_{DP}, A_H)$, $R(Z, K_{DP}, A_H)$, $R(K_{DP})$, $R(K_{DP}, Z_{DR})$,
 23 $R(Z, Z_{DR})$, and $R(Z)$. In Sect. 3.3 and 4.1, the statistical scores of $R(Z, Z_{DR}, K_{DP}, A_H)$ did not
 24 change significantly with respect to different Z_H and Z_{DR} biases. The results of the simulation
 25 and observations suggest that the accuracy of $R(Z, Z_{DR}, K_{DP}, A_H)$ is relatively weakly affected
 26 by errors in each polarimetric variable.

27

28 5 Conclusions

29 To improve polarimetric rainfall estimation and examine the candidates for an optimum
 30 rainfall relation using polarimetric variables observed from the Bislsan radar, the first
 31 polarimetric radar in Korea, a heavy rainfall case of 7 hours duration caused by low-pressure
 32 conditions on 25 August 2014 was analysed.



1 The theoretical approach to investigate the observed Z_{DR} quality used the relation between the
2 standard deviation of Z_{DR} and ρ_{hv} using the scan strategy parameters of the Bislsan radar.
3 The result showed that more samples were required to achieve the theoretical accuracy in Z_{DR} .
4 The best performance was obtained when a moving average Z_{DR} with window size of 9 gates
5 was applied to the rainfall estimation using $R(Z, Z_{DR})$ and to the calculation of Z_H bias. The
6 Z_{DR} quality check should be performed before using Z_{DR} for quantitative applications like
7 rainfall estimation and hydrometeor classification for the Bislsan radar. We also expect that
8 the light rain method for obtaining the Z_{DR} bias may be used as an alternative to the vertical
9 pointing scan method, because the rainfall estimation using this method performed well in our
10 case. Using DSD data for the calculation of Z_{DR} bias might give more accurate rainfall
11 estimation with $R(Z, Z_{DR})$.

12 Finally, the accuracy of $R(Z, Z_{DR}, K_{DP}, A_H)$ was not very sensitive to Z_{DR} and Z_H biases in both
13 observations and simulations. Thus $R(Z, Z_{DR}, K_{DP}, A_H)$ is expected to be less sensitive to Z_{DR}
14 and Z_H errors and could be used to estimate rainfall for heavy rainfall cases in Korea until an
15 accurate hydrometeor classification algorithm is developed.

16

17 **Acknowledgements**

18 The authors acknowledge the Ministry of Land, Infrastructure, Transport and the Korea
19 Meteorological Administration for providing radar data and AWS data for this work. The
20 authors acknowledge Prof. V. N. Bringi at Colorado State University, who provided the
21 scattering simulation code. The authors also acknowledge Prof. A. C. Illingworth at Reading
22 University who provided valuable comments on Z_{DR} data quality. This research was funded
23 by the Korea Meteorological Industry Promotion Agency under Grant KMIPA 2015-1050.

24



1 **References**

- 2 Andsager, K., Beard, K. V., and Laird, N. S.: A laboratory study of oscillations and axis ratios
3 for large raindrops”, *Journal of the Atmospheric Sciences*, 55, 208-226, 1999.
- 4 Austin, P. M.: Relation between measure radar reflectivity and surface rainfall, *Monthly*
5 *Weather Review*, 115, 1053-1070, 1987.
- 6 Beard, K. V. and Chuang, C.: A new model for the equilibrium shape of raindrops, *Journal of*
7 *the Atmospheric Sciences*, 44, 1509-1524, 1987.
- 8 Bringi, V. N. and Chandrasekar, V.: The polarimetric basis for characterizing precipitation.
9 *Polarimetric Doppler weather radar: Principles and applications*, Cambridge University Press:
10 Cambridge, UK, pp. 378-533, 2001.
- 11 Bringi, V. N., Chandrasekar, V., Hubbert, J., Gorgucci, E., Randeu, W., and Schoenhuber, M.:
12 Raindrop size distribution in different climate regimes from disdrometer and dual-polarized
13 radar analysis, *Journal of Atmospheric Science*, 60, 354-365, 2003.
- 14 Campos, E., Zawadzki, I.: “Instrumental uncertainties in Z-R relations”, *Journal of Applied*
15 *Meteorology*, 36, 1088-1102, 2000.
- 16 Cifelli, E. V., Chandrasekar, V., Lim, S., Kennedy, P. C., Wang, Y., and Rutledge, S. A.: A
17 new dual-polarization radar rainfall algorithm: Application in Colorado precipitation events,
18 *Journal of Atmospheric and Oceanic Technology*, 28, 352-364, 2011.
- 19 Giangrande, S. E. and Ryzhkov, A. V.: Estimation of rainfall based on the results of
20 polarimetric echo classification, *Journal of Climate and Applied Meteorology*, 47, 2445-2462,
21 2008.
- 22 Gorgucci, E., Scarchilli, G., and Chandrasekar, V.: A procedure to calibrate multiparameter
23 weather radar using properties of the rain medium. *IEEE Transactions on Geoscience and*
24 *Remote Sensing*, 37: 269–276, 1999.
- 25 Huang, G.-J., Bringi, V. N., and Thurai, M.: Orientation angle distributions of drops after 80
26 m fall using a 2D-video disdrometer, *Journal of Atmospheric Oceanic Technology*, 25, 1717-
27 1723, 2008.



- 1 Jang, M., Lee, D., and You, C.: Z-R relationship and DSD analyses using a POSS disdrometer.
- 2 Part I: Precipitation cases in Busan, *Journal of the Korean Meteorological Society*, 40, 557-
- 3 570, 2004.
- 4 Keat, W. J., Westbrook, C., Illingworth, A.: Measurements of the co-polar coefficient in
- 5 rainfall and retrieval of the drop size distribution, 37th AMS on radar conference, 2015.
- 6 Mishchenko, M. I., Travis, L. D., and Mackowski, D. W.: T-matrix computations of light
- 7 scattering by nonspherical particles: A review, *Journal of Quantitative Spectroscopy and*
- 8 *Radiative Transfer*, 55, 535-575, 1996.
- 9 Loffler-Mang, M., Joss, J.: An optical disdrometer for measuring size and velocity of
- 10 hydrometeors, *J. Atmos. Oceanic. Technol.*, 17, 130-139, 2000
- 11 Marks, D. A., Wolff, D. B., Carey, L. D., and Tokay, A.: Quality control and calibration of
- 12 the dual-polarization radar at Kwajalein, RMI. *Journal of Atmospheric and Oceanic*
- 13 *Technology*, 28: 181–196, 2011.
- 14 May, P., Keenan, T. D., Zrníc, D. S., Carey, L., and Rutledge, S.: Polarimetric radar
- 15 measurement of tropical rain at 5-cm wavelength, *Journal of Applied Meteorology*, 38, 750-
- 16 765, 1999.
- 17 Ryzhkov, A. V. and Zrníc, D. S.: Discrimination between rain and snow with a polarimetric
- 18 radar, *Journal of Applied Meteorology*, 37, 1228-1240, 1998.
- 19 Ryzhkov, A. V. and Zrníc, D. S.: Assessment of rainfall measurement that uses specific
- 20 differential phase, *Journal of Applied Meteorology*, 35, 2080-2090, 1996.
- 21 Ryzhkov, A. V., Schuur, T. J., Burgess, D. W., Heinselman, P. L., Giangrande, S. E., and
- 22 Zrníc, D. S.: The Joint Polarization Experiment: Polarimetric rainfall measurements and
- 23 hydrometeor classification, *Bulletin of the American Meteorological Society*, 86, 809-824,
- 24 2005a.
- 25 Ryzhkov, A. V., Giangrande, S. E., Melnikov, V. M., and Schuur, T. J.: Calibration issues of
- 26 dual-polarization radar measurements. *Journal of Atmospheric and Oceanic Technology*, 22:
- 27 1138–1155, 2005b.
- 28 Ryzhkov, A., Dieberich, M., Zhang, P., and Simmer, C.: Potential utilization of specific
- 29 attenuation for rainfall estimation, mitigation of partial beam blockage, and radar networking,
- 30 *Journal of Atmospheric and Oceanic Technology*, 31, 599-619, 2014.



- 1 Sheppard, B. E.: Measurement of raindrop size distributions using a small Doppler radar,
2 Journal of Atmospheric and Oceanic Technology, 7, 255-268.
- 3 Suk, M., Nam, K., Kim, Y., and Oh, S.: Estimation of quantitative rain intensity from radar
4 reflectivities using a wind probability matching method, Journal of the Korean Meteorological
5 Society, 41, 123-138, 2005.
- 6 Trabal, J. M., V. Chandrasekar, E. Gorgucci and D. J. McLaughlin, 2009: Differential
7 reflectivity(ZDR) calibration for CASA radar network using properties of the observed
8 medium, Geoscience and Remote Sensing Symposium,2009 IEEE International,IGARSS
9 2009 (Volume:2) II-960-II963.
- 10 You, C., Lee, D., Jang, M., Uyeda, H., Shinoda, T., and Kobayashi, F.: Characteristics of
11 rainfall systems accompanied with Changma front at Chujado in Korea, Asia-Pacific Journal
12 of Atmospheric Sciences, 46, 41-51, 2010.
- 13 You, C., Lee, D., Jang, M., Seo, K., Kim, K., and Kim, B.: The characteristics of rain drop
14 size distributions using a POSS in Busan area, Journal of the Korean Meteorological Society,
15 40, 713-724, 2004.
- 16 You, C.-H., Lee, D.-I., Kang, M.-Y.: Rainfall estimation using specific differential phase for
17 the first operational polarimetric radar in Korea, Advances in Meteorology, vol. 2014, Article
18 ID 41317, 10 pages, doi:10.1155/2014/413717, 2014.
- 19 You, C.-H. and Lee, D.-I.: Algorithm development of the optimum rainfall estimation using
20 polarimetric variables in Korea. Advances in Meteorology, vol. 2015, Article ID 395937, 15
21 pages, doi:10.1155/2015/395937, 2015a.
- 22 You, C.-H. and Lee, D.-I.: Decadal variation in raindrop size distributions in Busan, Korea,
23 Advances in Meteorology, vol. 2015, Article ID 329327, 8 pages, 2015,
24 doi:10.1155/2015/329327, 2015b.
- 25 Vivekanandan, J., Zrníc, D. S., Ellis, S. M., Oye, R., Ryzhkov, A. V., and Straka, J.: Cloud
26 microphysics retrieval using S-band dual-polarization radar measurements, Bulletin of the
27 American Meteorological Society, 80, 381-388, 1999.
- 28 Waterman, P. C.: Symmetry, unitarity, and geometry in electromagnetic scattering, Physical
29 Review D, 3, 825-839, 1971.



1 Wilson, J. W. and Brandes, E. A.: Radar measurement of rainfall-A summary, Bulletin of the
2 American Meteorological Society, 60, 1048-1058, 1979.

3
4
5
6
7
8
9
10
11
12
13
14
15
16
17
18
19
20
21
22
23
24
25
26



1 Table 1. Polarimetric radar rainfall relations used in this study.

Relations		Relations	
R(Z)	$R=0.017Z^{0.714}$	R(K _{DP})	$R=61.5K_{DP}^{0.908}$
R(A _H)	$R=3409A_H^{1.02}$	R(Z,Z _{DR})	$R=0.0148Z^{0.818}Z_{DR}^{-3.72}$
R(K _{DP} ,Z _{DR})	$R=82.2K_{DP}^{0.855}Z_{DR}^{-1.977}$	R(Z,K _{DP} ,A _H)	$R=17211Z^{-0.027}K_{DP}^{0.62}A_H^{0.65}$
R(Z,Z _{DR} ,K _{DP} ,A _H)		$R=4502Z^{-0.014}Z_{DR}^{-0.389}K_{DP}^{0.486}A_H^{0.653}$	

2

3 Table 2. Statistics of the comparison of hourly rainfall amount between R(Z,Z_{DR}) and gages.

Relation	Z _H bias source	Z _{DR} bias source	RMSE	NE	CC
$R=0.0148Z^{0.818}Z_{DR}^{-3.72}$	Observed Z _{DR}	Observed Z _{DR}	17.2	0.66	0.77
		mZ _{DR}	9.2	0.56	0.95
	mZ _{DR}	Observed Z _{DR}	15.2	0.53	0.77
		mZ _{DR}	7.4	0.45	0.95

4

5 Table 3. Same as Table 2 but for R(Z,Z_{DR},K_{DP},A_H).

Relation	Z _H bias source	Z _{DR} bias source	RMSE	NE	CC
$R=4502Z^{-0.014}Z_{DR}^{-0.389}K_{DP}^{0.486}A_H^{0.653}$	Observed Z _{DR}	Observed Z _{DR}	5.2	0.30	0.95
		mZ _{DR}	5.2	0.30	0.95
	mZ _{DR}	Observed Z _{DR}	5.3	0.30	0.95
		mZ _{DR}	5.4	0.31	0.95

6

7

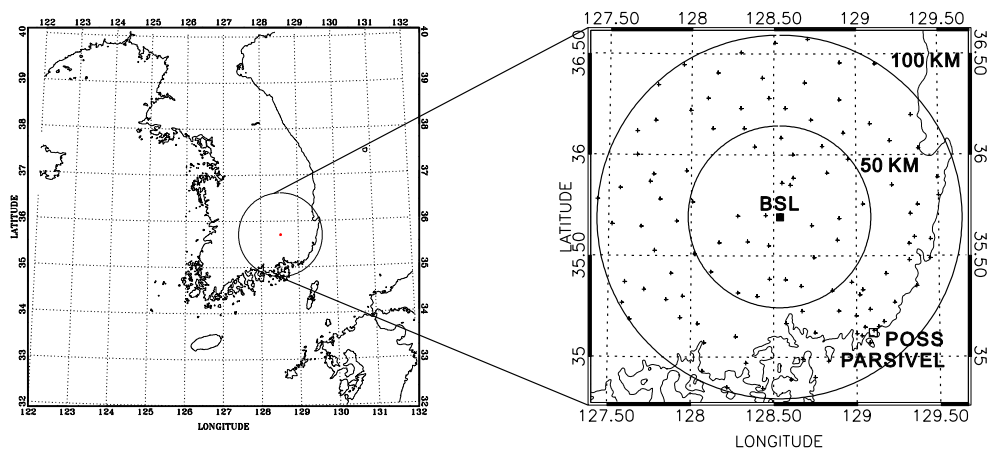
8

9

10



1



2

3 Figure 1. Location of Bislan radar (solid rectangle), the POSS and PARSIVEL disdrometer
4 (open rectangle), and rain gages (plus signs) distributed within 100 km of the radar. The
5 circles are at 50 and 100 km from the radar.

6

7

8

9

10

11

12

13

14

15

16

17

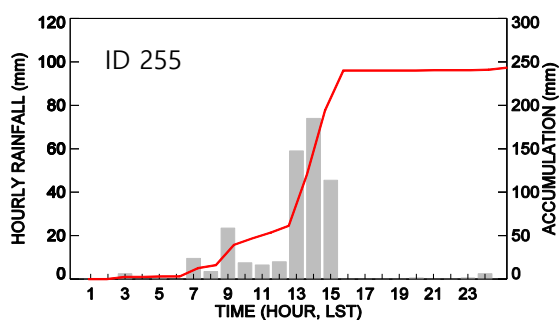
18

19



1

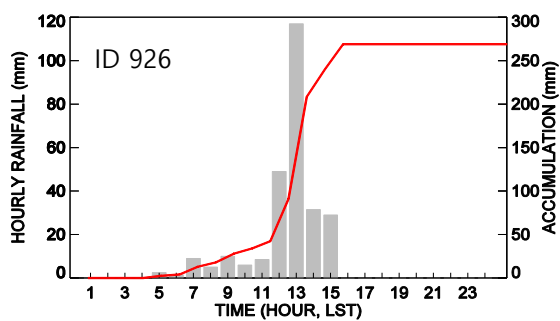
(a)



2

3

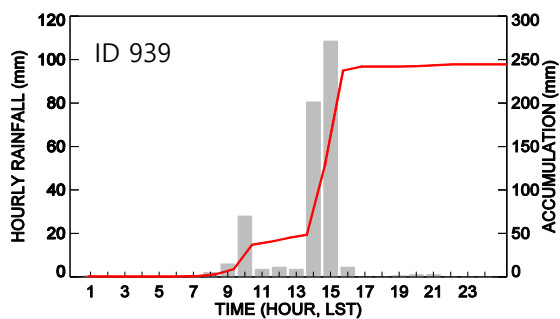
(b)



4

5

(c)



6

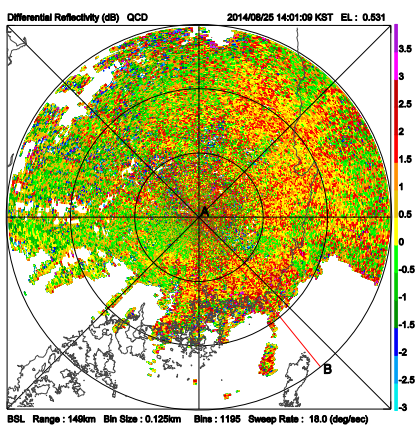
7 Figure 2. Time series of hourly rainfall (gray bars) and accumulation (red line) from the three
8 gages that recorded the highest rainfall (a) ID 255, (b) ID 926, (c) ID 939.

9



1

(a)

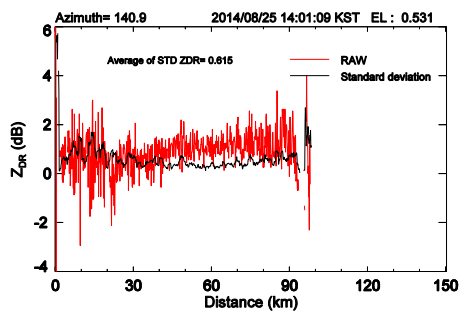


2

3

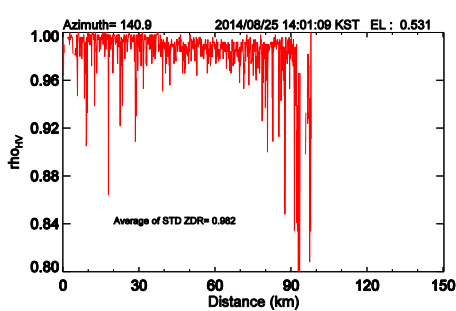
4

(b)



5

(c)



6 Figure 3. (a) Distribution of Z_{DR} within the radar coverage, (b) the radial profile of Z_{DR} and (c)
7 cross correlation along the line A–B in (a) at 1401 LT 25 August 2014.

8

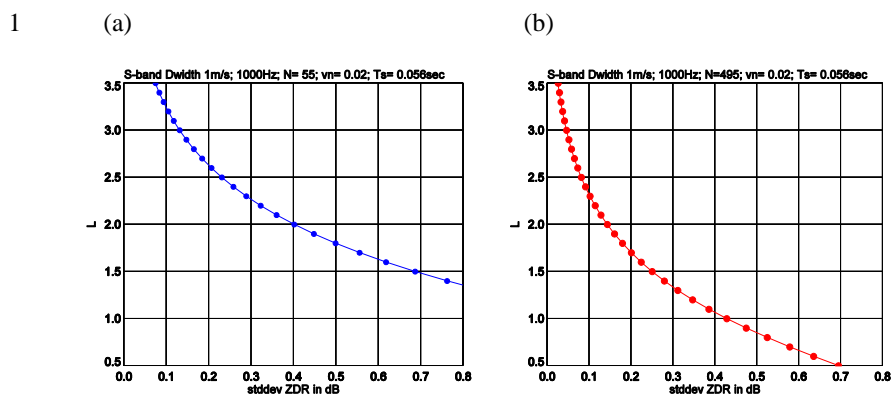
9

10

11

12

13



2

3 Figure 4. Theoretical relation between standard deviation of Z_{DR} and cross correlation using
4 (a) the scan configuration of the Bislan radar. Dwell time is 56 ms, number of samples is 55,
5 normalized Doppler width is 0.02; (b) same as (a) but for 495 samples.

6

7

8

9

10

11

12

13

14

15

16

17

18

19

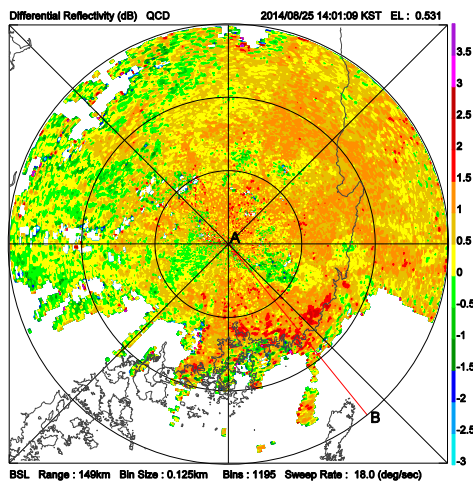
20

21



1

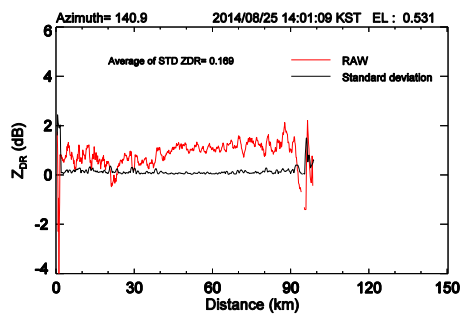
(a)



2

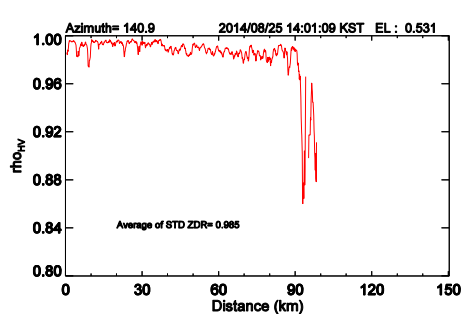
3

(b)



4

(c)



5 Figure 5. Same as Fig. 3 but for moving averages of Z_{DR} .

6

7

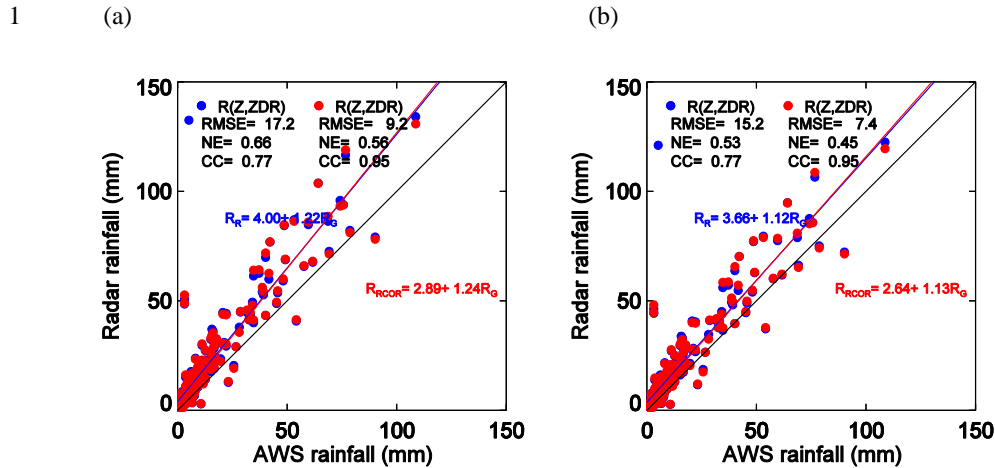
8

9

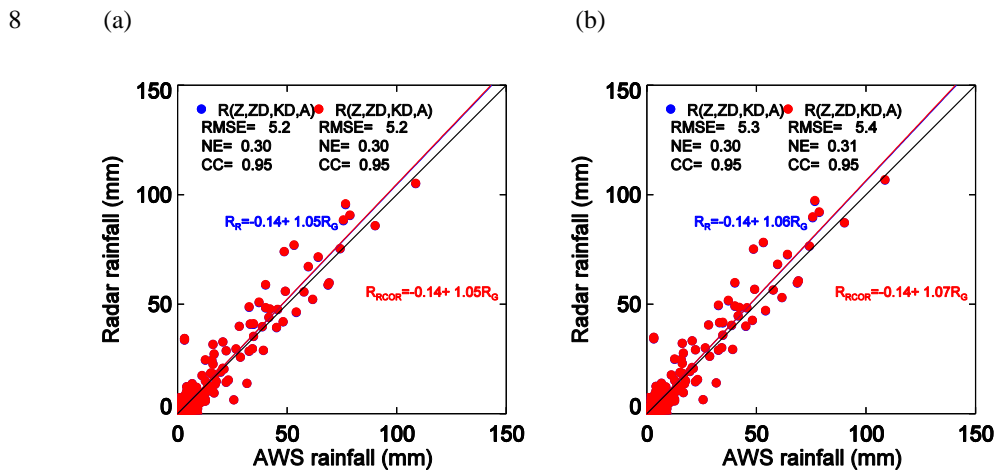
10

11

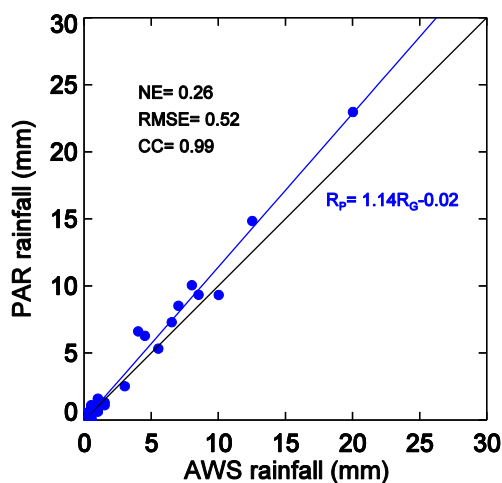
12



2
 3 Figure 6. Scatter plot of 1 hour rainfall obtained by R(Z,Z_{DR}) against gage rainfall. (a) Radar
 4 rainfall was calculated using Z_H bias calculated from observed Z_{DR} bias and Z_{DR} biases
 5 calculated from observed Z_{DR} (blue full circles) and mZ_{DR} (red full circles), (b) same as (a)
 6 but for Z_H bias calculated from mZ_{DR}.



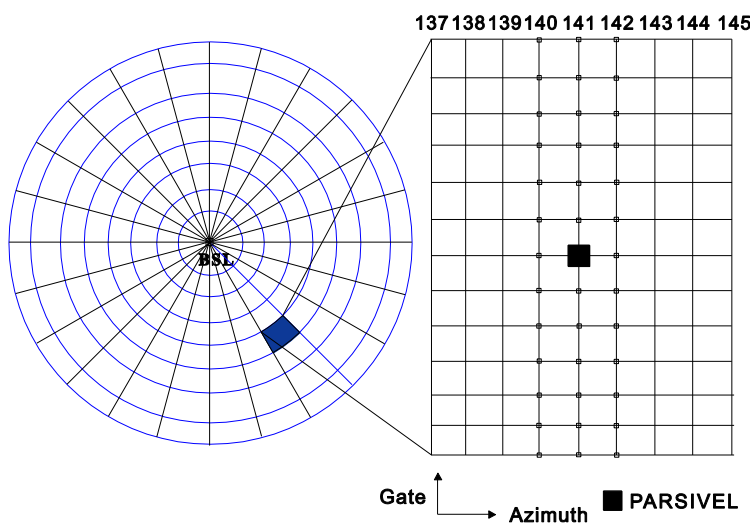
9
 10 Figure 7. Same as Fig. 6 but for radar rainfall obtained by R(Z,Z_{DR},K_{DP},A_H).
 11



1

2 Figure 8. Scatter plot of 10 min rainfall amount measured by PARSIVEL and gage for 24
 3 hours.

4

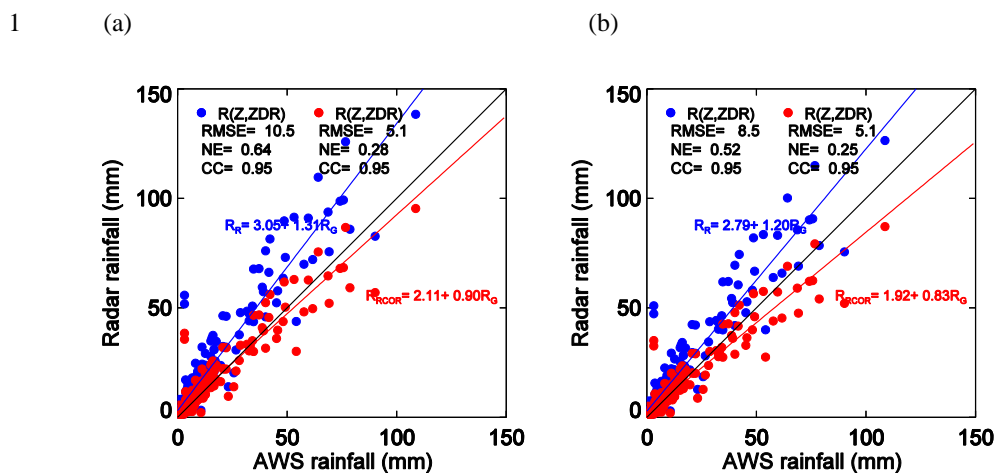


5

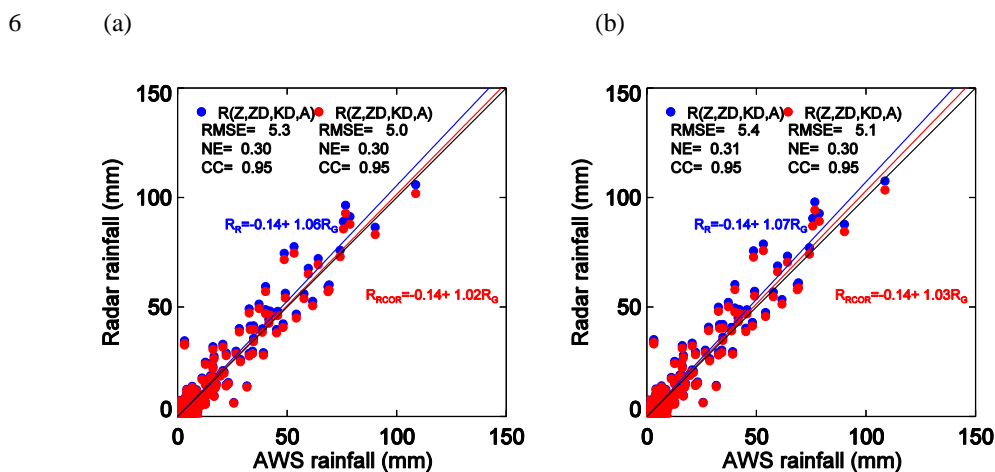
6

7 Figure 9. Schematic diagram for the comparison of radar and PARSIVEL Z_{DR} . The numbers
 8 refer to azimuth angle.

9

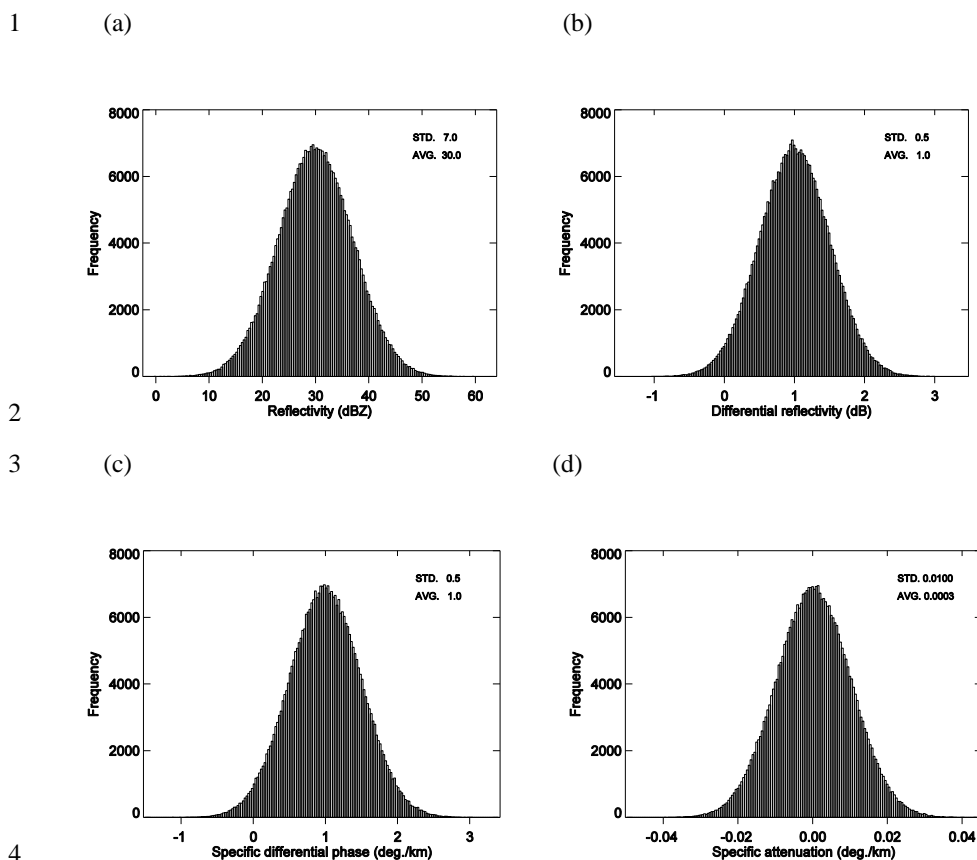


2
 3 Figure 10. Same as Fig. 6 but for Z_{DR} biases determined by comparison between radar and
 4 PARSIVEL.



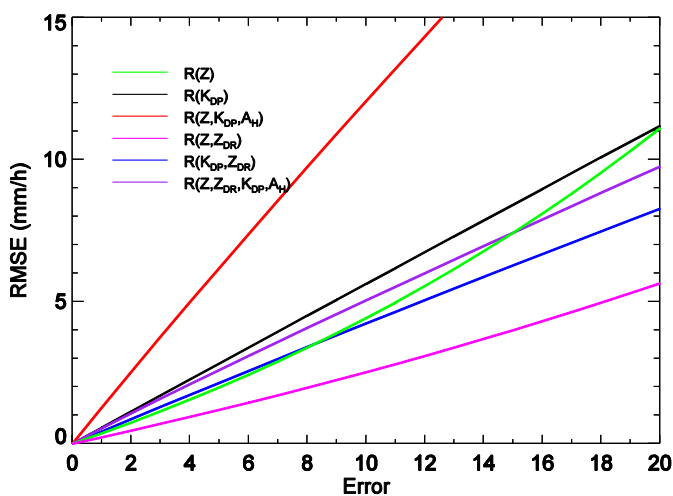
7
 8 Figure 11. Same as Fig. 7 but for Z_{DR} biases determined by comparison between radar and
 9 PARSIVEL.

10
 11



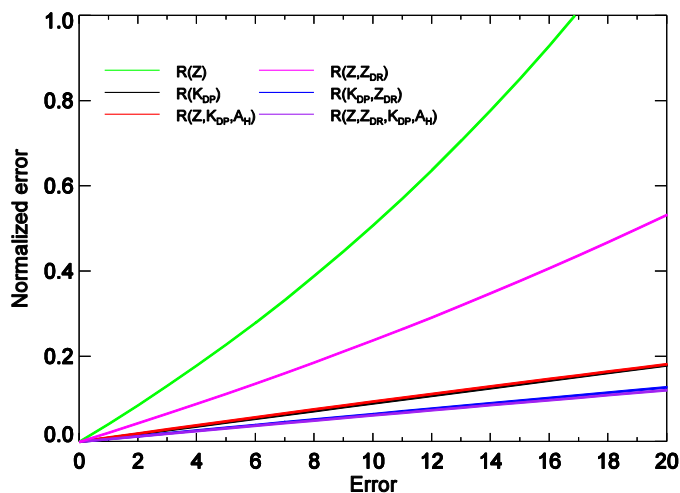


1 (a)



2

3 (b)



4

5 Figure 13. Distribution of (a) RMSE and (b) NE with generated errors for different rainfall
 6 relations. Magenta, black, red, green, blue, and purple lines show RMSE and NE obtained
 7 from the rainfall relations $R(Z)$, $R(K_{DP})$, $R(Z, K_{DP}, A_H)$, $R(Z, Z_{DR})$, $R(K_{DP}, Z_{DR})$, and
 8 $R(Z, Z_{DR}, K_{DP}, A_H)$, respectively.